**OVRO-LWA Memo No. 16**

# Calculation of LWA Antenna Beams and Close Packing Effects

David Woody
California Institute of Technology

2015 October 20

Submitted 2023 January 23

To cite this memo in another document, use:
"OVRO-LWA Memo 16, 2015 Oct 20, http://tauceti.caltech.edu/LWA/lwamemos.html "

# Calculation of LWA Antenna Beams and Close Packing Effects

David Woody, October 20, 2015

## 1. Introduction

Improving our knowledge of the LAW antenna beam pattern and the effect of nearby antennas is an important step to improving the calibration and image fidelity of the OVLWA (Owens Valley Long Wavelength Array). Previous LWA studies carried out a MoM (method of moments) calculation of the beam pattern and produced analytic approximations to the E- and H-plane beam patterns which are currently used for the image processing [LWA memos 175 and 178]. A MoM model has been developed using the GRASP and HFSS analysis programs to calculate other beam properties, such as the beam pattern in non-principle directions and Stokes parameters, and to explore the effect of nearby antennas and ground plate configurations.

## 2. LWA antenna model

Figures 1 and 2 show the GRASP antenna model used for the calculations. The dipole leafs were modeled as conducting plates. The outer dimensions of the plates match the as constructed antennas. The ground shield was a 3 m x 3 m perfect reflector below the antenna. The use of plates instead of the rectangular tube construction simplified the model construction and decreased the memory size and computation time required for the calculations and should have only a small effect on the accuracy of the results. The calculations were carried out in the usual time reversed method of treating the receiver as a transmitter.

Several ground configurations have been analyzed including a single antenna in free space with no ground, an infinite perfectly conducting ground, and various sizes of perfectly conducting ground shield patches and conducting patches on a 30 m dia lossy disk to simulate dirt. The lossy ground is 5 m thick with a permittivity of 2, permeability of 1 and loss tangent of 2. The size of the disk was limited by the memory on my laptop and computation time. Changing the disk size and electrical properties had only a small effect on the beam pattern above ~10 deg from the horizon but did effect the beam at the horizon and the finite size allowed radiation to propagate in the negative direction. The driving point impedance in the GRASP model was critically dependent on the details of the model at the apex shown in fig. 2. It was difficult to arrive at a model that was simple enough to model and also produce the same driving point impedance that the LWA MoM modeling produced. The final GRASP model had roughly the correct frequency dependent driving point impedance and coupling efficiency to the sky. The beam calculations used a 50 ohm source to drive the leafs aligned along the X-axis while the Y-axis leafs were shorted to the ground plane at the top of the mast. The HFSS model had only one set of “dipole” leafs oriented along the X-axis direction and matched the LWA stated driving point impedance with a simple generator source driving the two leafs.

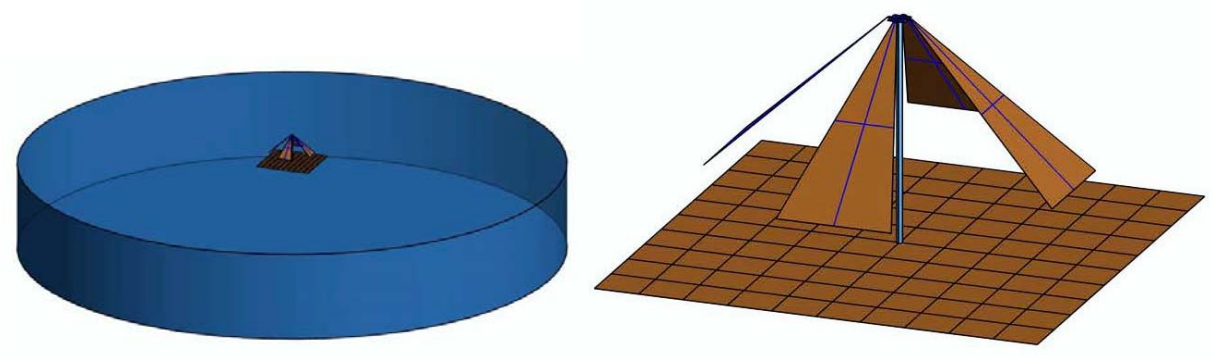

Fig. 1. Single LWA antenna. The left panel shows the antenna on the 30 m dia by 5 m thick lossy ground. The right panel shows the four leafs and ground reflector.

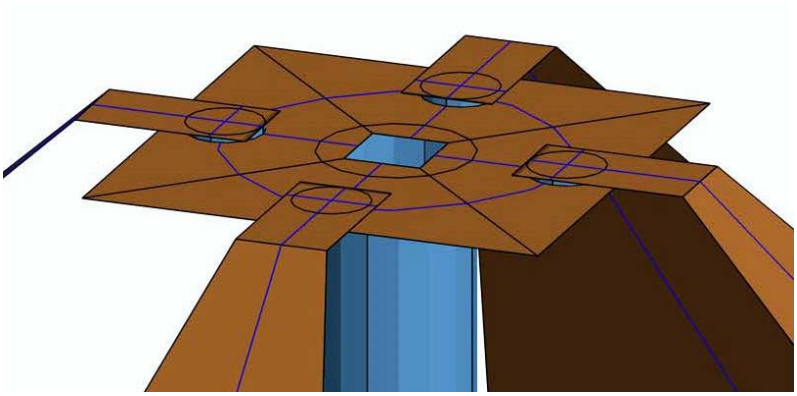

Fig. 2. Close up of the antenna apex and feed.

## 3. Single antenna calculations

The antenna beam pattern and cross-polarization properties are critically dependent on the ground plane configuration. The calculations start with the ideal case of an antenna in free space with no ground plane and progresses to an ideal infinite ground plane followed by more realistic models with finite ground shields and lossy dirt. The far-fields complex voltage patterns were calculated in Ludwig's 3rd polarization coordinate system,

$$\widehat{E_{co}} = \hat{\theta}\,\cos\emptyset - \hat{\emptyset}\,\sin\emptyset$$

$$\widehat{E_{cx}} = \hat{\theta}\,\sin\emptyset + \hat{\emptyset}\,\cos\emptyset.$$

$\widehat{E_{co}}$ is a good match to the nominal polarization for a dipole antenna near zenith. (In HFSS the corresponding coordinate vectors are L3X and L3Y.) As Larry D'Addario pointed out, it is the Stokes parameters that are most important for characterizing astronomical telescope beams. The four Stokes parameters are calculated using

$$I = |E_{co}|^2 + |E_{cx}|^2$$

$$Q = |E_{co}|^2 - |E_{cx}|^2$$

$$U = 2\,Re(\,E_{co}{E_{cx}}^*)$$

$$V = -2\,Im(\,E_{co}{E_{cx}}^*)$$

and are plotted along with the power in the polarization components, $P_{CO}$ and $P_{CX.}$ The beam pattern is calculated along cuts in the two principle planes and diagonal plane (0 45 and 90 azimuth directions) at frequencies of 20, 50 and 80 MHz.

### 3.1 Antenna in free space

Both HFSS and GRASP models were used to calculate the beam for a naked antenna in free space. Figures 3, 4 and 5 shows the calculated beams using the HFSS analysis model. The total radiated power is moderately well behaved with minimums at the horizon, +-90 deg zenith angles, although 80 MHz beam only has a modest decrease in gain at the horizon. More importantly for measuring polarization, the Stokes V is very large along the diagonal 45 deg azimuth cut near the horizon. At 50 and 80 MHz in the 45 deg azimuth the beam is essentially 100% circularly polarized near the horizon. The antenna geometry shown in fig. 1 shows how this circular polarization is generated. Away from the principle planes the two leafs of the antenna are at an ~90 deg angle and there is a relative propagation time delay which produces the necessary phase shift to generate circular polarization.

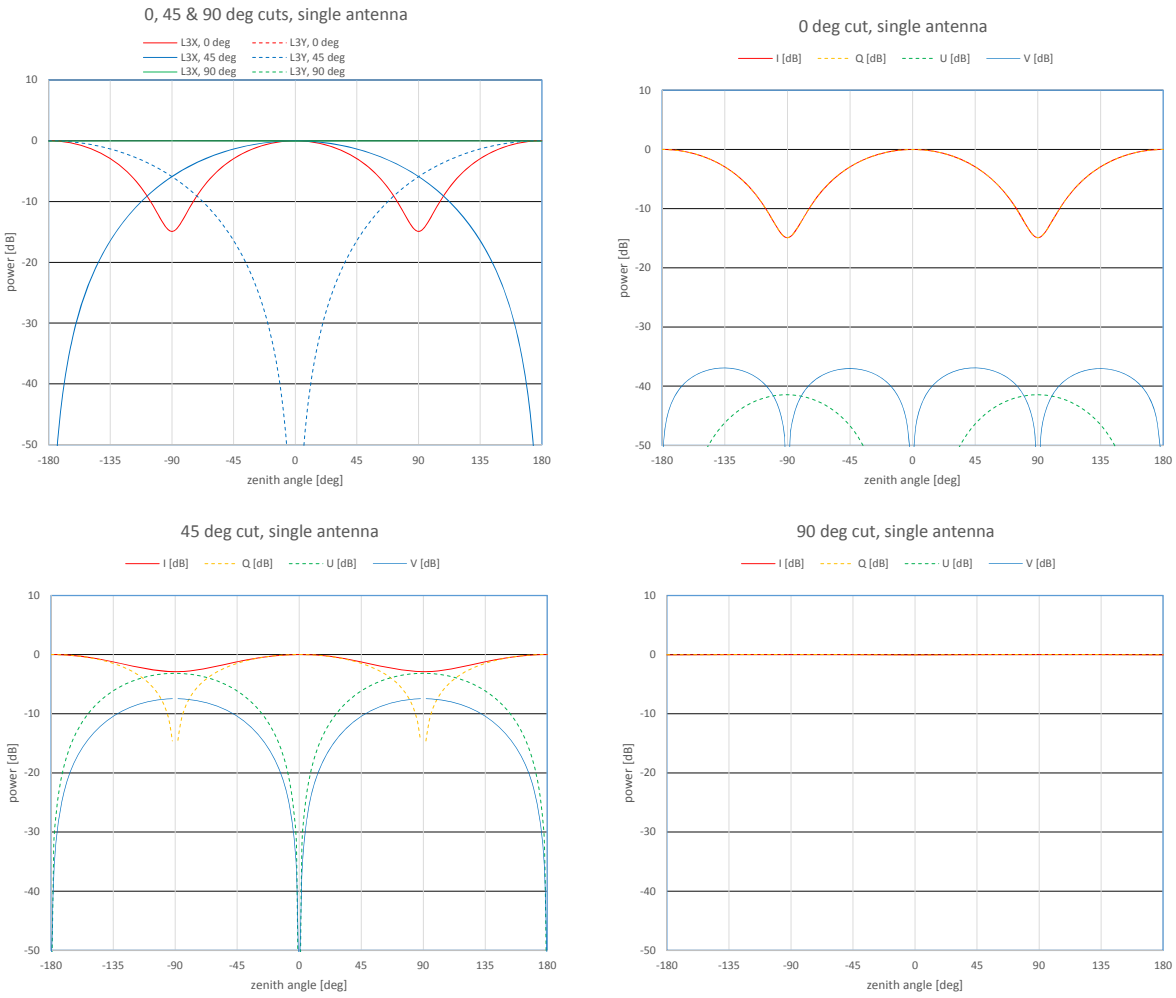


Fig. 3. Antenna beam in free space at 20 MHz calculated using HFSS. The upper left panel shows the power in the two linear polarizations for beam cuts at 0, 45 and 90 deg azimuths. The top right shows the Stokes parameters along the 0 deg azimuth while the lower left and right panels show the Stokes parameters along the 45 deg and 90 azimuth planes respectively. The horizontal axes is the zenith angle from -180 deg (back lobe) to 0 deg (zenith) and to +180 deg (back lobe again). Lines that don't show up are either directly on top of an existing line or off scale below -50 dB. The plots are normalized to unity at zenith for L3X.

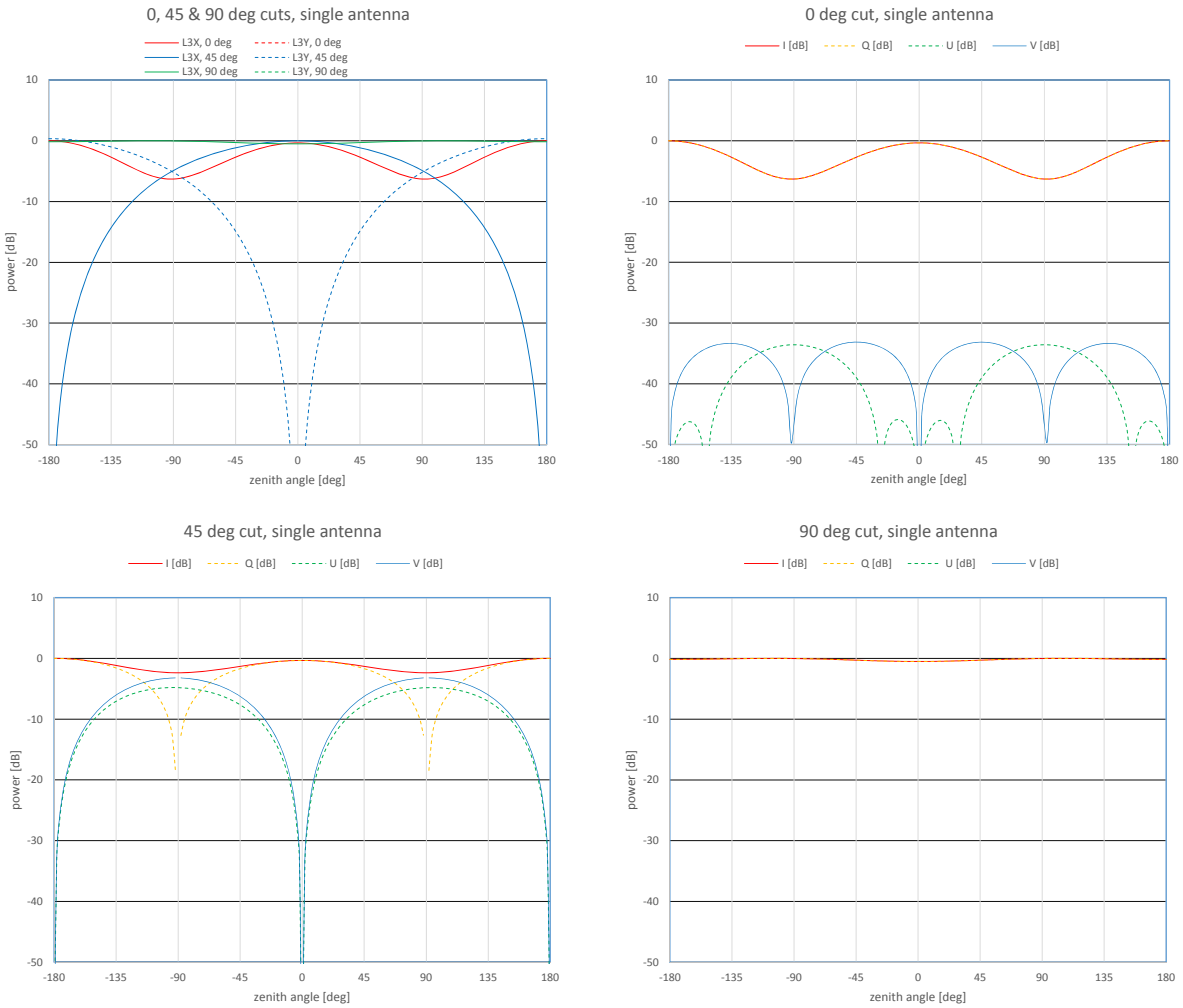


Fig. 4. Antenna beam in free space at 50 MHz calculated using HFSS. Same format as fig. 3.

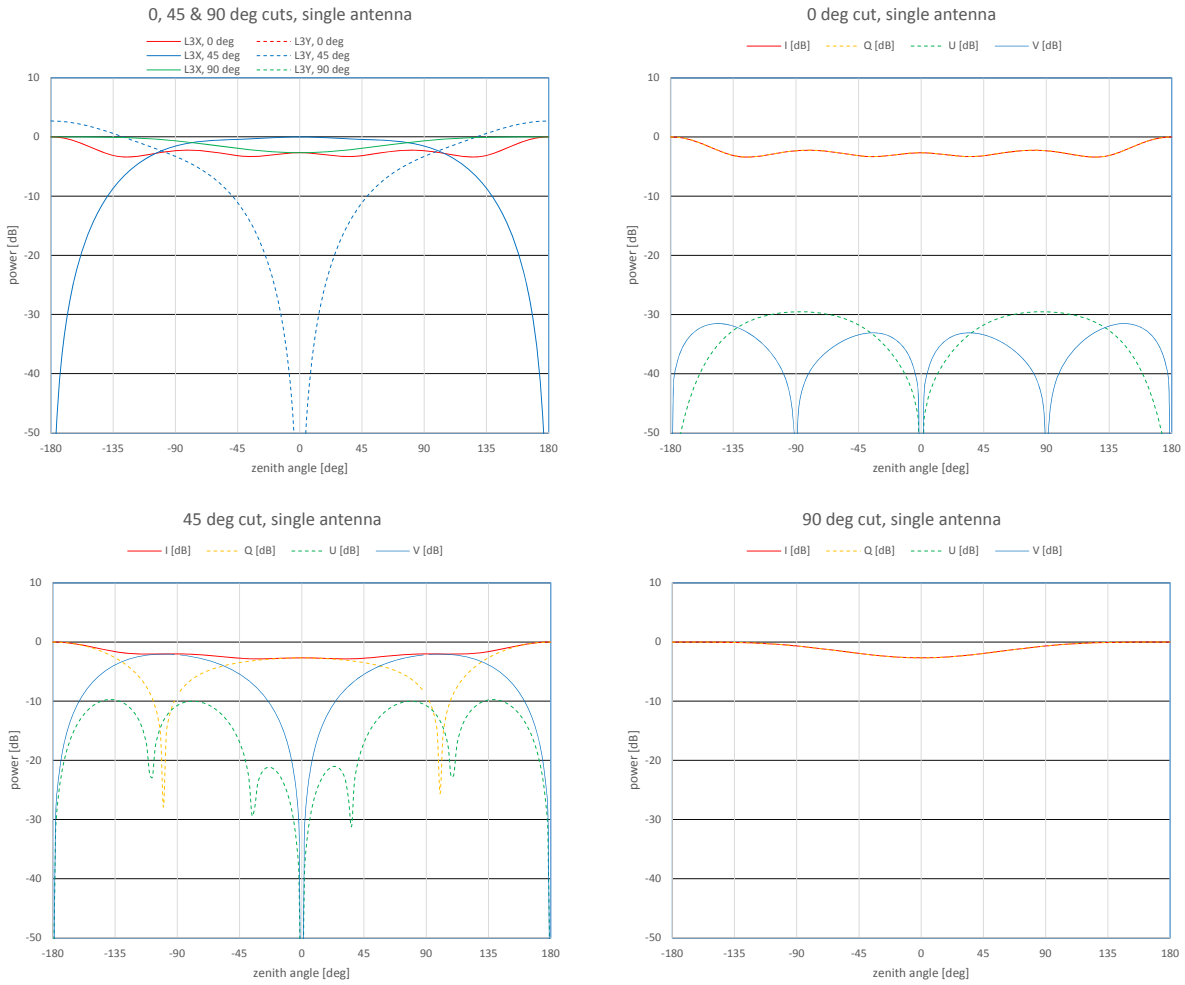


Fig. 5. Antenna beam in free space at 80 MHz calculated using HFSS. Same format as fig. 3.

Figures 6 and 7 compare the calculated 50 MHz beams using the HFSS and GRASP analysis programs. The maximum difference for the I, Q and V polarizations is <6% of the beam at zenith while the U polarizations agree to better than 1%. The agreement is significantly better at 20 MHz with a maximum difference of 1% for V and significantly worse at 80 MHz where the maximum difference for V is 17%. The details of the two models at the feed point or apex differ and this may cause the differences in the calculated beams. Further work is required to resolve which program is more accurate. It should be noted that both programs produced the expected beam pattern with no circular polarization for a simple straight wire dipole antenna.

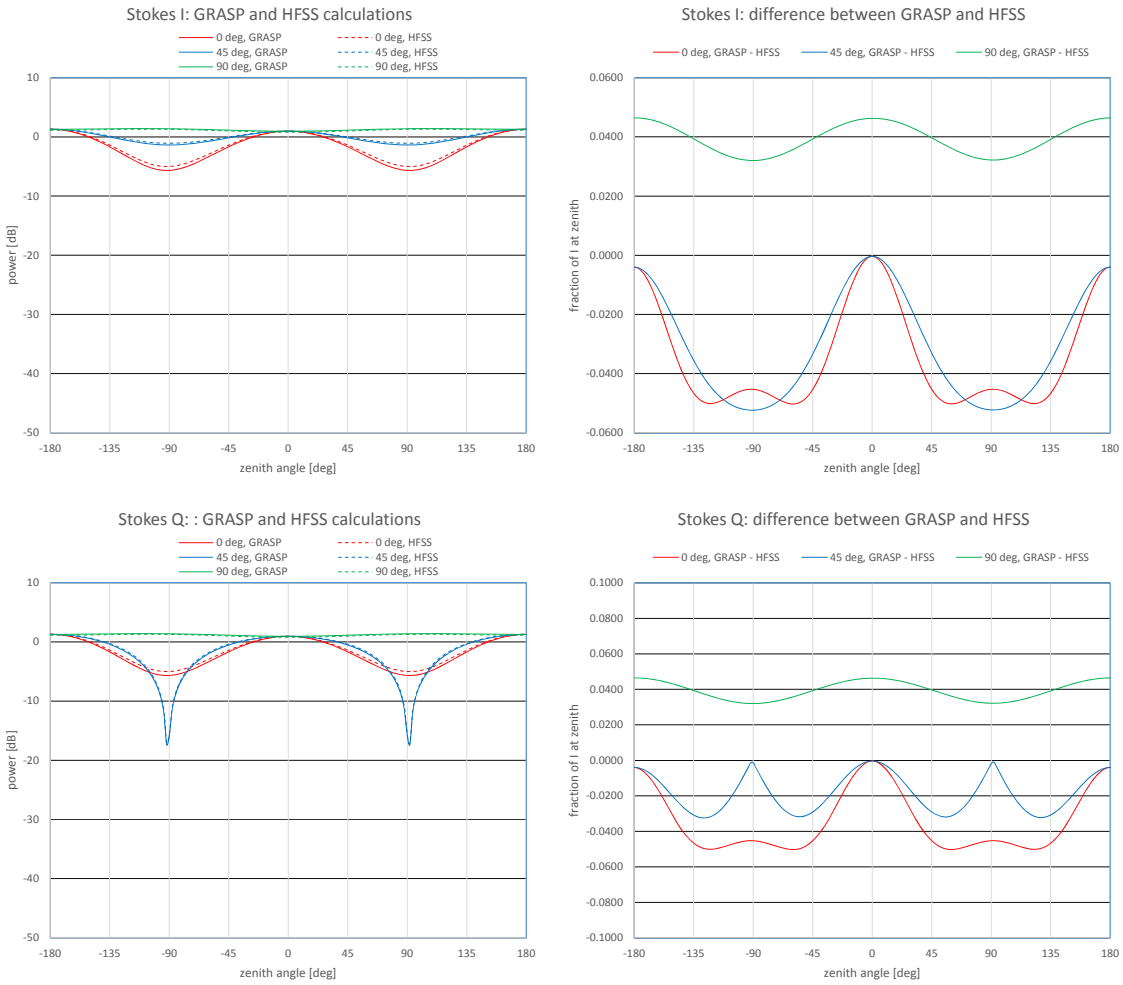


Fig. 6. Comparison of the GRASP and HFSS calculations of I and Q beam polarization at 50 MHz. The left panels show the calculated beams and the right panels show the difference between the two programs as a fraction of I at zenith.

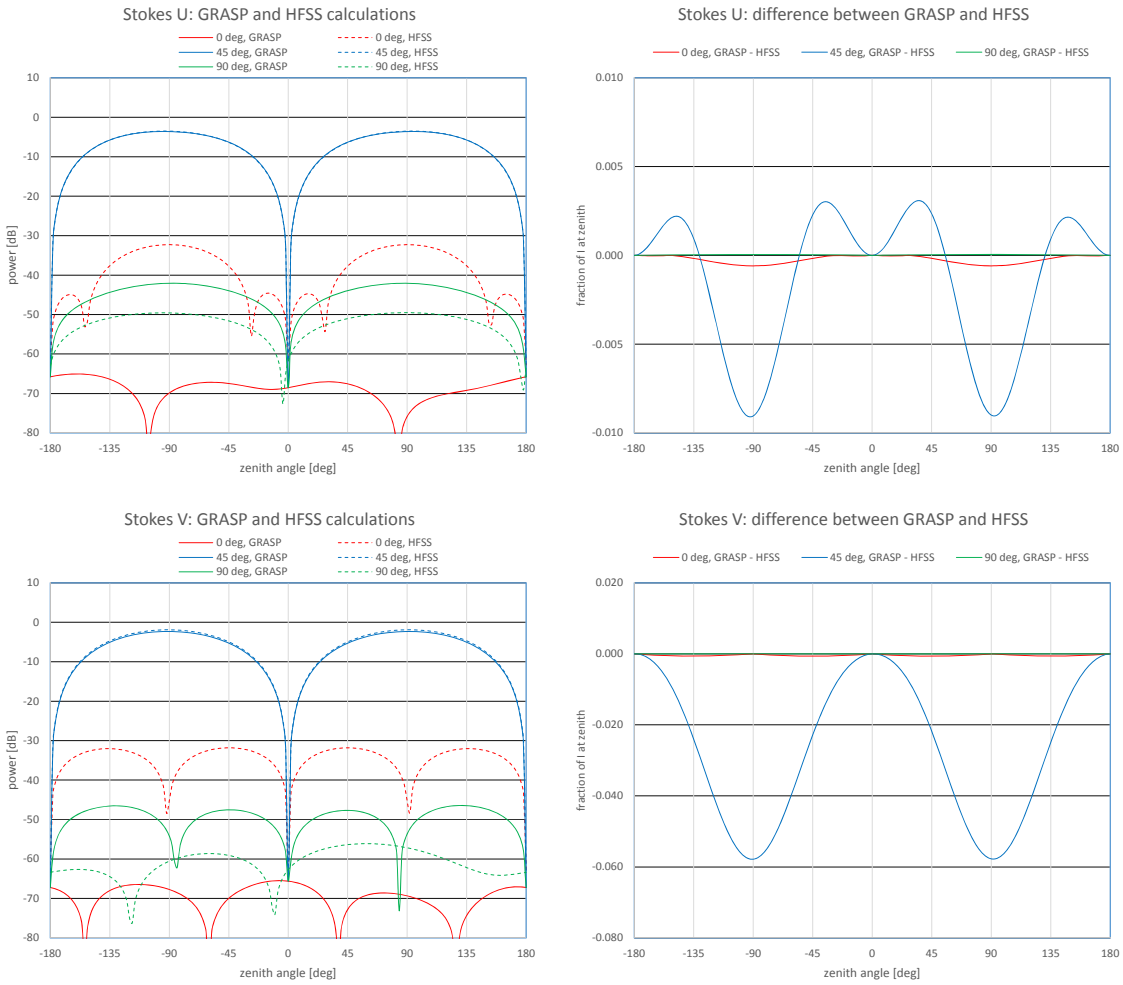


Fig. 7. Comparison of the GRASP and HFSS calculations of U and V beam polarization at 50 MHz. Same format as fig. 6.

## 3.2 Antenna with infinite conducting ground plane

Adding an finite perfectly conducting ground plane will increase the gain at zenith and change the beam polarization. The beams for this case are shown in fig. 8, 9 and 10. The addition of the perfect infinite ground plane greatly decreased the Stokes V polarization for the 45 deg azimuth beam cut. At 20 MHz Stokes V peak is only -40 dB at 60 deg zenith angle but degrades to -19 dB at 50 MHz and to -8 dB at 80 MHz. It was expected that the reflection symmetry from the infinite ground plane would have eliminated Stokes V at all frequencies and angles. Thinking that the problem may be with the model at the apex where the two leafs are driven, I decreased the separation of the two terminals from 132 mm to 20 mm which has essentially no effect on the beam Stokes parameters. The residual Stokes V shown in figs. 8, 9 and 10 could be a figment of the HFSS analysis model and the 50 MHz Stokes V is consistent with the differences between the GRASP and HFSS calculations for the free space case shown in fig. 7. Varying the convergence criteria and looking at the symmetry of the results for the HFSS analysis indicate that the results are robust at the -30 dB level or better. Unfortunately the GRASP MoM package does not allow inclusion of an infinite perfectly conducting ground plane for comparison to the HFSS results, but using a 200 m x 200 m perfectly conducting ground shield produced nearly the same Stokes I in all beam cuts and Stokes of V in 45 deg azimuth plane down to ~70 deg zenith angle.

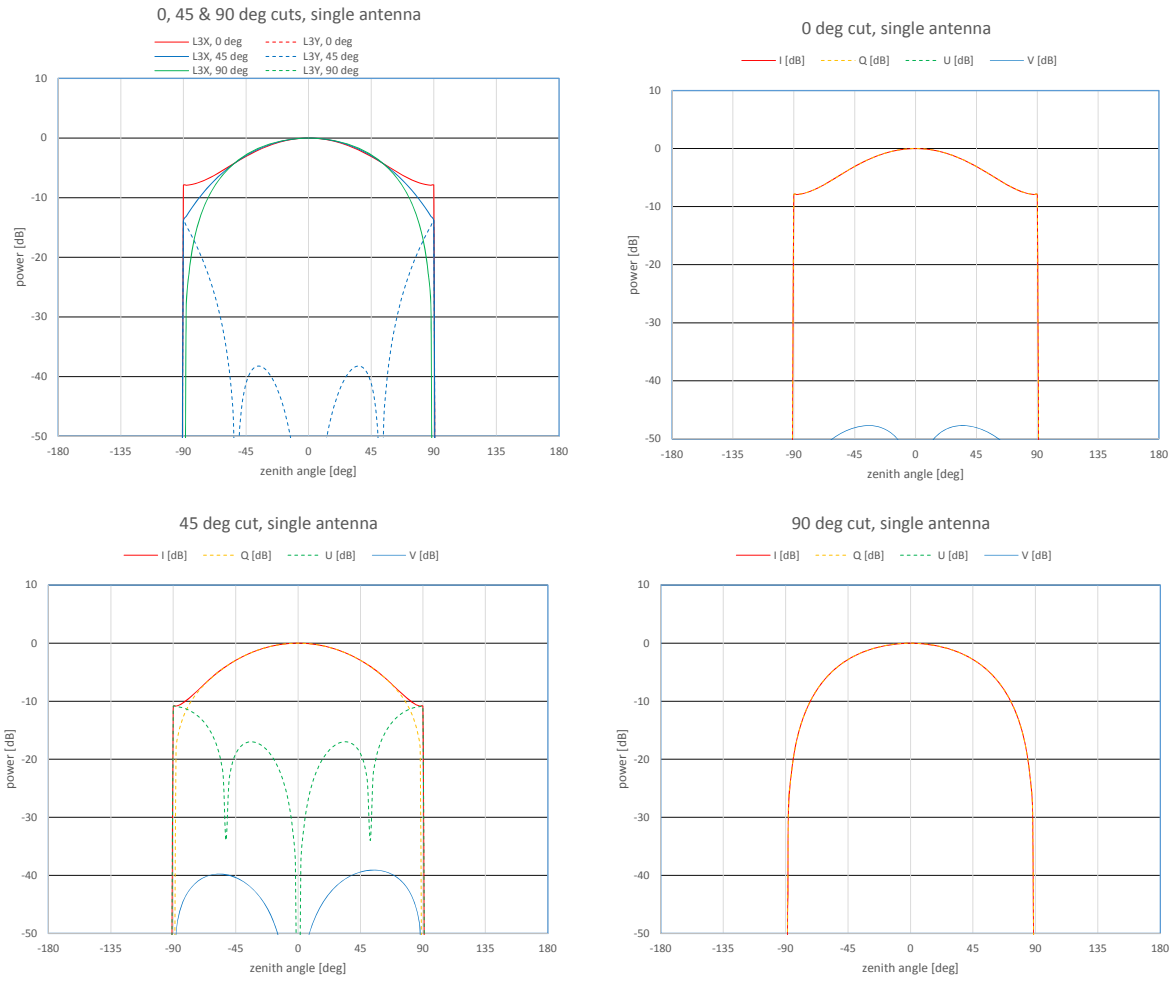


Fig. 8. Antenna beam with infinite perfectly conducting ground plane at 20 MHz calculated using HFSS. Same format as fig. 3.

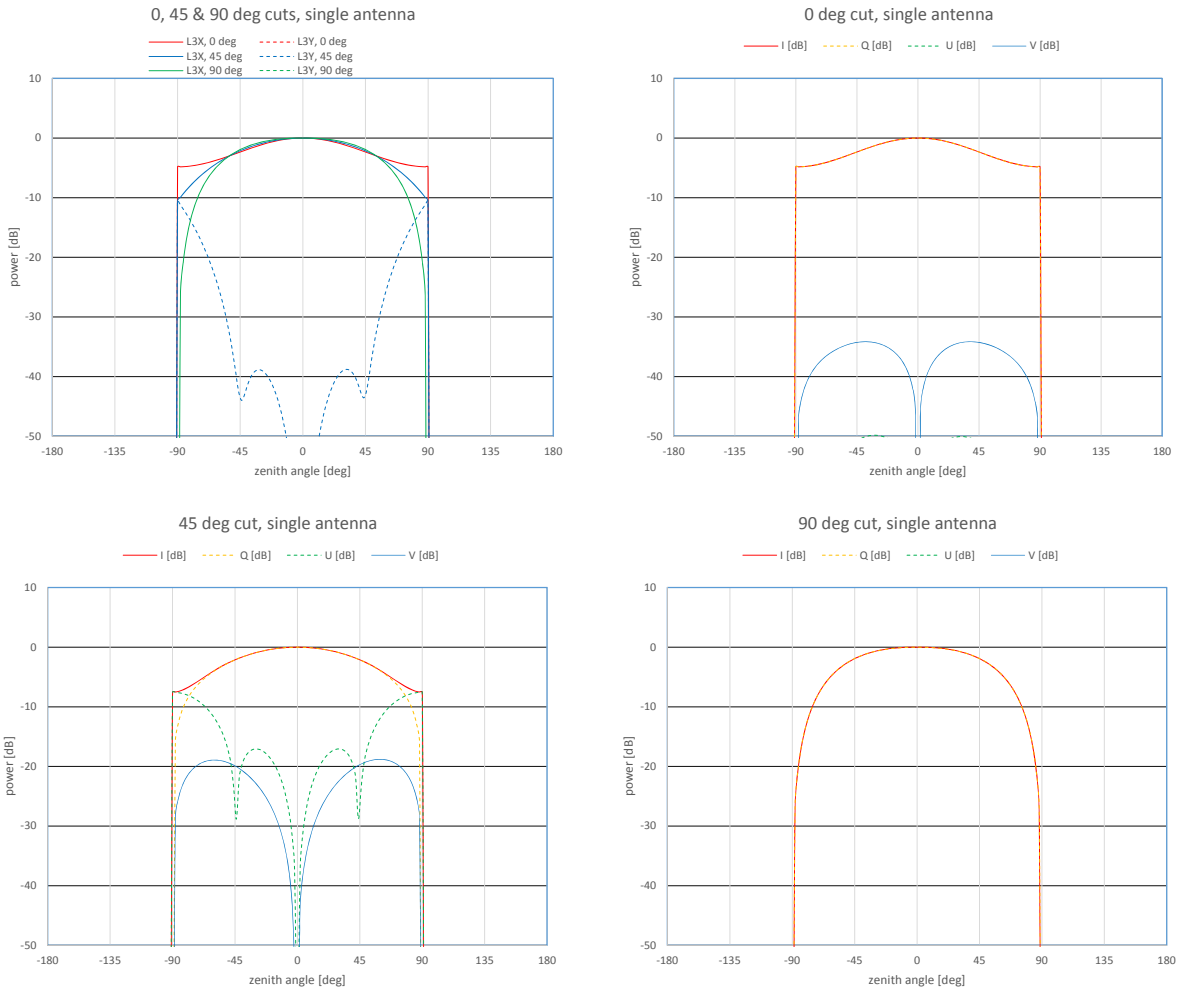


Fig. 9. Antenna beam with infinite perfectly conducting ground plane at 50 MHz calculated using HFSS. Same format as fig. 3.

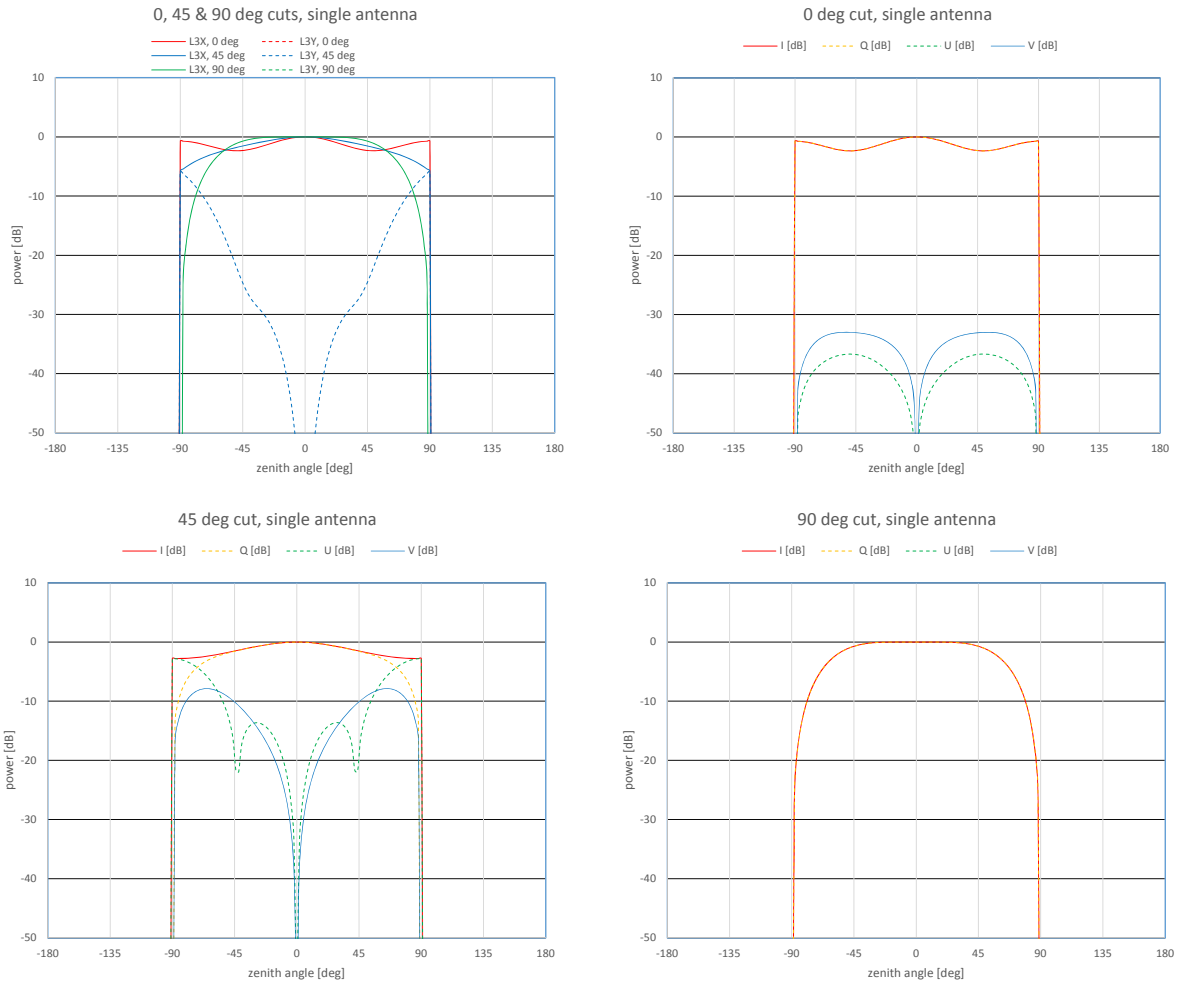


Fig. 10. Antenna beam with infinite perfectly conducting ground plane at 80 MHz calculated using HFSS. Same format as fig. 3.

## 3.3 Antenna with finite ground shield

The as built OVLWA and NMLWA use a 3 m x 3 m open mesh ground shield. This ground shield was modeled as a perfectly conducting patch in both GRASP and HFSS and in GRASP a 30 m dia by 5 m thick with a loss tangent of 2 and permittivity of 2 was included to simulate the dirt ground. (The size of the lossy disk was limited by the 16 GB memory size on my laptop computer.) The GRASP results for this configuration are shown in figs. 11, 12 and 13. These results appear to be robust at the -40 dB level. The Stokes V, as might be expected, is between the extremes seen for the antenna in free space and on an infinite ground plane.

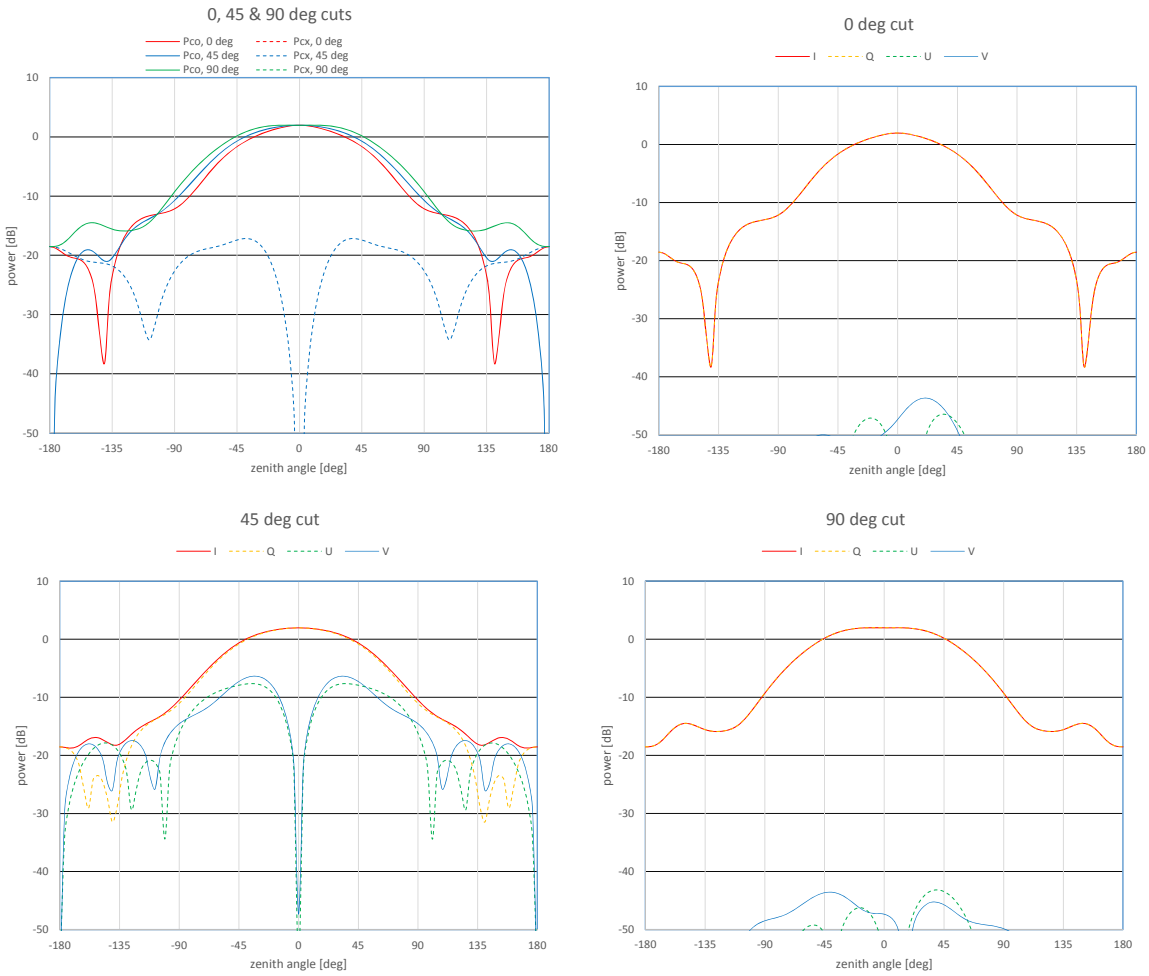


Fig. 11. Antenna beam with 3 m x 3 m ground shield and 30 dia lossy ground at 20 MHz calculated using GRASP. Same format as fig. 3 but with gain relative to an isotropic transmitter.

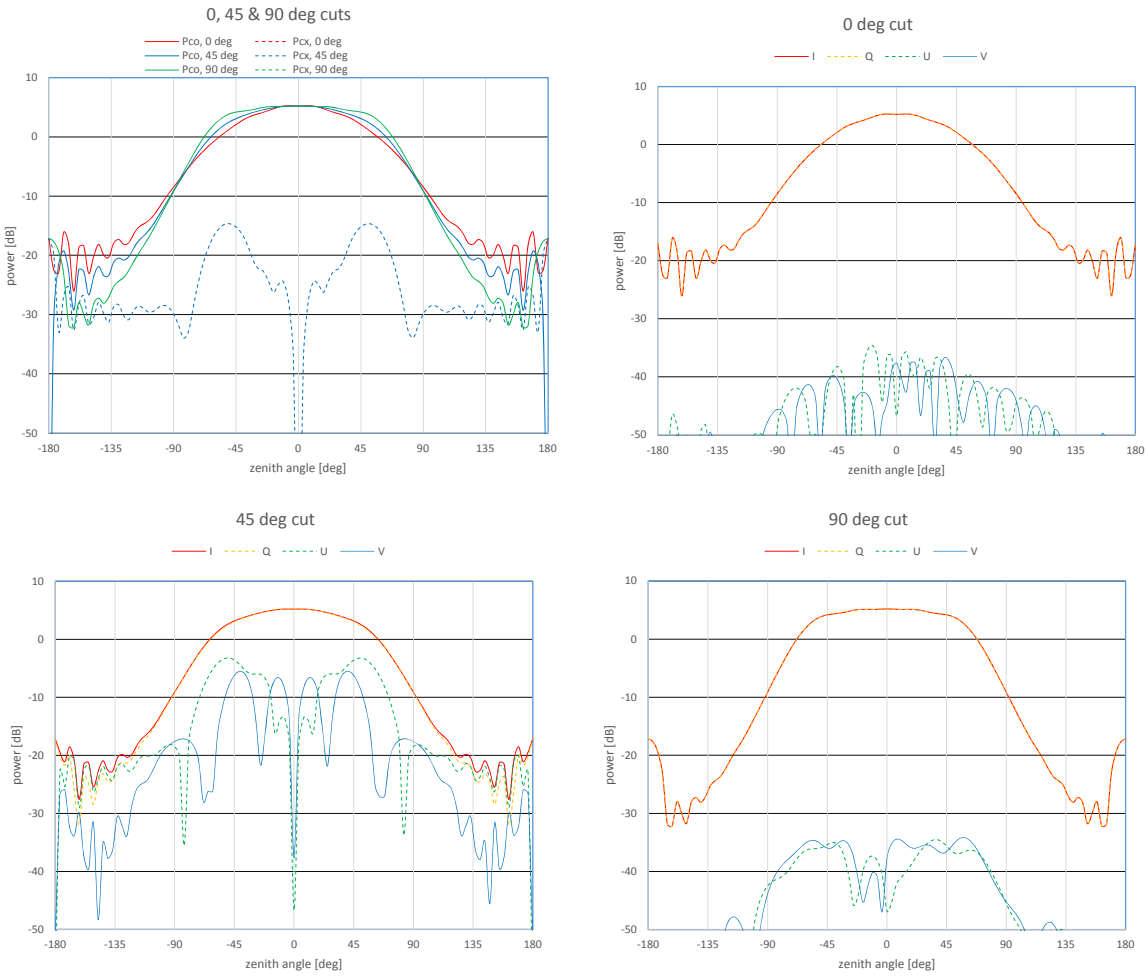


Fig. 12. Antenna beam with 3 m x 3 m ground shield and 30 dia lossy ground at 50 MHz calculated using GRASP. Same format as fig. 11.

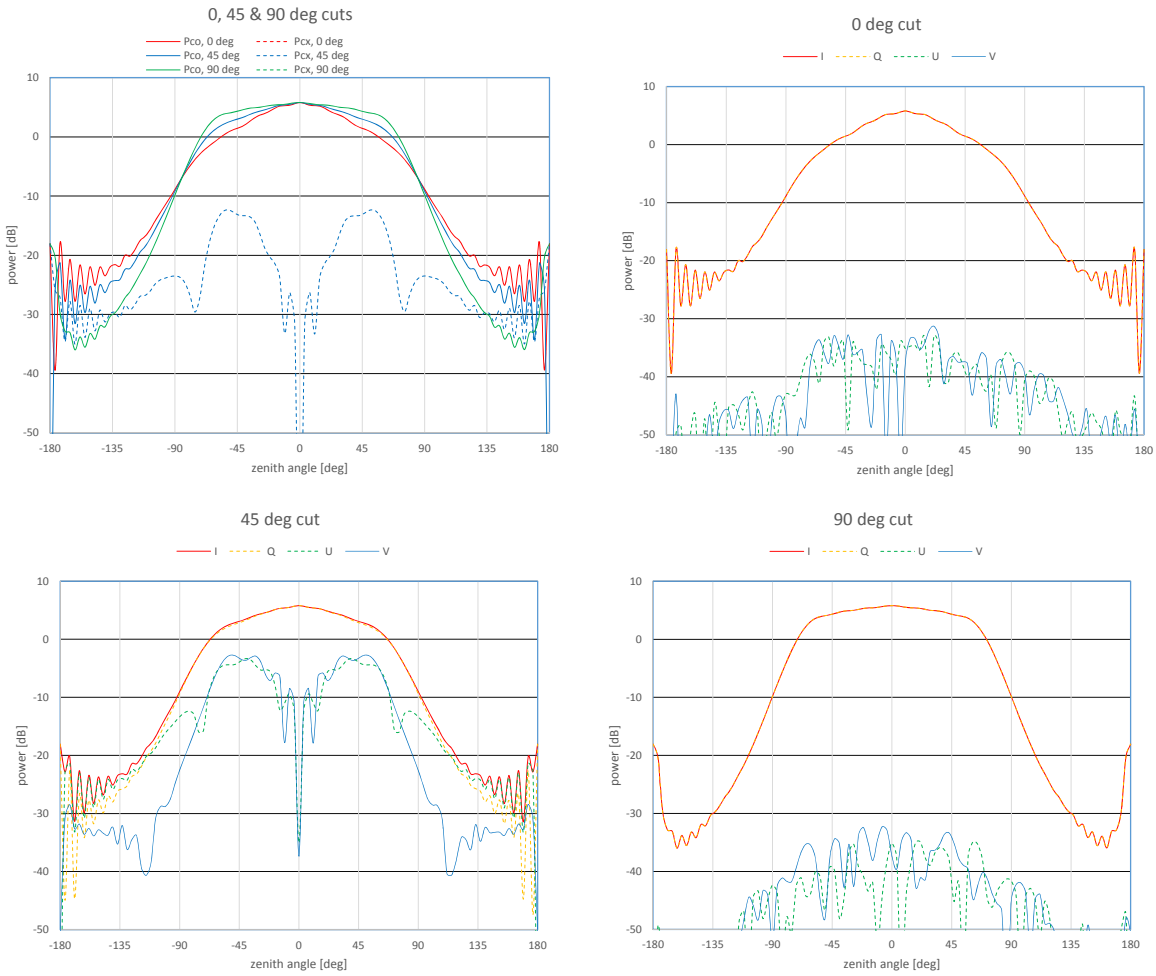


Fig. 13. Antenna beam with 3 m x 3 m ground shield and 30 dia lossy ground at 80 MHz calculated using GRASP. Same format as fig. 11.

James Lamb pointed out that the finite size of the ground shield could adversely affect the polarization of the beam and indeed adding a 3 m x 3 m ground shield to a simple straight wire dipole produces significant Stokes V in the diagonal plane. Thus the finite sized ground shield can jeopardize the linear polarization purity of any antenna design. This can be visualized by treating the ground shield as a mirror and when you look at the antenna off zenith and away from the principle planes you will see image of the real antenna clipped asymmetrically at the edge of mirror. This asymmetry, which increases as the zenith angle increases or as the ground shield shrinks, produces circular polarization.

Another issue with the ground shield is that resonant like ripple starts to show up in the beam cuts as the shield dimensions become larger than one wavelength. This is just starting to show up for the 3 m x 3 m ground shield at 80 MHz and is very prominent when a 10 m x 10 m ground shield is used as seen in fig. 14. This will further complicate gain calibration strategies and short term source variability measurements. It will also have an impact on measurements of broad spectral and spatial features.

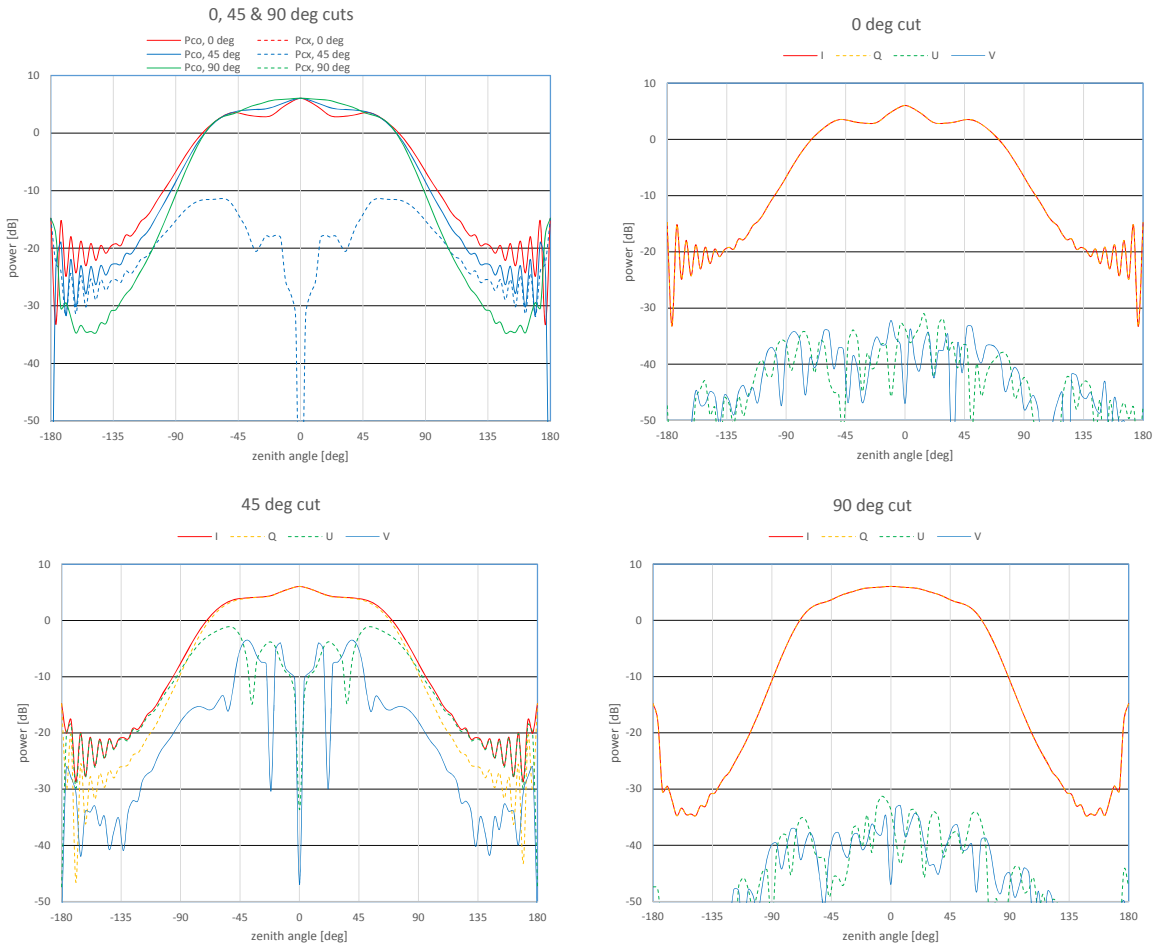


Fig. 14. Antenna beam with 10 m x 10 m ground shield and 30 dia lossy ground at 80 MHz calculated using GRASP. Same format as fig. 11.

The calculations presented here are for an idealized antenna. Fabrication and installation imperfections could cause deviations from the calculated beam patterns. The fabrication of the inverted V dipole leafs and the installation of the antennas should be precise enough to not produce a measureable difference in the beam pattern from one station to the next. But the ground shield in not precisely made or installed. It is cut from rolls of fencing material and laid out on the uneven desert ground. Thus the reflected symmetry for the image dipoles will not be ideal and there are tilts in the ground plane that could be as large as several degrees. This would shift the position and shape of the beam on the sky. This effect needs to be further explored in the calculations.

Another area that could lead to deviations from the calculated behavior is the coupling from the leafs to the amplifiers. The mismatch can be large and hence may not be well matched between the two branches of the FEE board. The GRASP calculations for a 20% voltage imbalance yielded a Stokes V of -20 to -15 dB in the 90 deg azimuth plane compared to a balanced drive which produced no Stokes V. The Stokes V in the 0 deg azimuth plane was still essentially zero and in the 45 deg azimuth plane the Stokes V changed by 1 to 2 dB and became slightly asymmetric.

### 3.4 Polarization orthogonality of E-W and N-S beams

Measuring polarization with an interferometer relies critically on the correlation or visibility between one polarization receiver on antenna and the complementarily polarized receiver on the second antenna, i.e. the E-W signal on the first antenna correlated with the N-S signal on the second antenna. Ideally even if the beams do not have a nice ideal linear polarization state, the polarization states for the E-W and N-S beams should be orthogonal so that an unpolarized signal would produce zero correlation between for the E-W to N-S signals. The correlations between the E-W and N-S beams for antennas with 3 m x 3 m ground shield and 30 m dia lossy ground are plotted in fig. 16. The beams have excellent orthogonality on the principle planes but correlation in the diagonal 45 deg azimuth plane can be as large as 30%. (This degree of cross-correlation could have been expected from the amount of Stokes V seen in figs. 11, 12 and 13 but significant Stokes V in both beams does not necessarily produce correlation. The circular polarization component in the E-W and N-S beams could have had opposite rotation, i.e. left circular vs. right circular, and still produce zero correlation.) The significant correlation between the E-W and N-S beams will require accurate calibration of the cross polarization terms to detect weakly polarized sources.

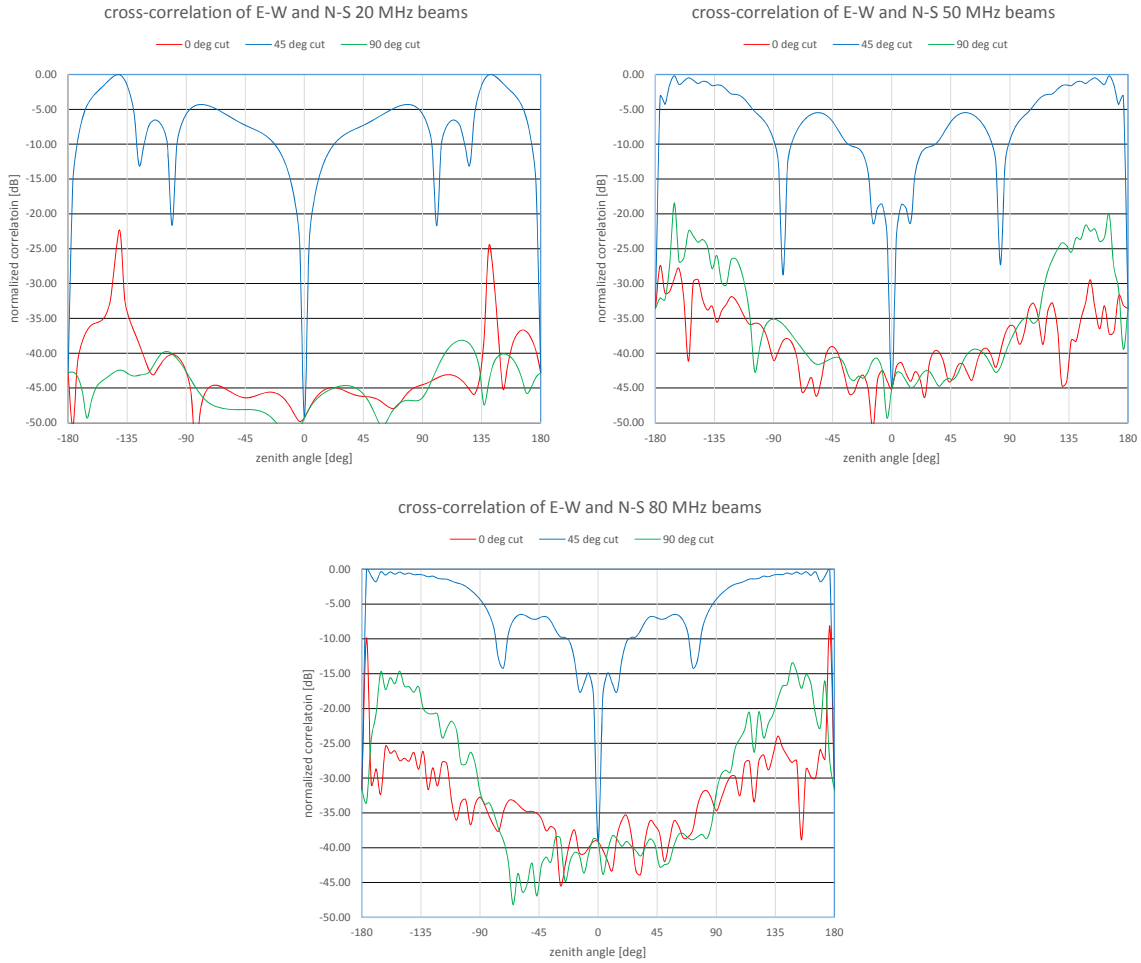


Fig. 15. Orthogonality of the E-W and N-S beams at 20, 50 and 80 MHz. The antennas model has a 3 m x 3 m ground conducting shield and 30 m dia lossy dirt ground.

There is another mechanism for producing correlation between the E-W and N-S beams. Figure 16 shows the current density in the leafs when the E-W leafs are treated as a transmitter in the GRASP model. The

currents in the East and West leafs induce currents in the East and West sides of North and South leafs. Nominally the phases of these induced currents would cancel at the terminals but an unbalanced front end for the East and West leafs would produce a net coupling into the N-S pair. This would not be important if the front ends were matched loads but there is actually a large mismatch to the input amplifiers, especially at low frequencies. Thus a large fraction of the input signal is reflected back into the leafs and if the reflected signal from the East and West leafs are not balanced the reflected signal will induce correlated signals in the N-S leaf pair. Further calculations are required to quantify this effect.

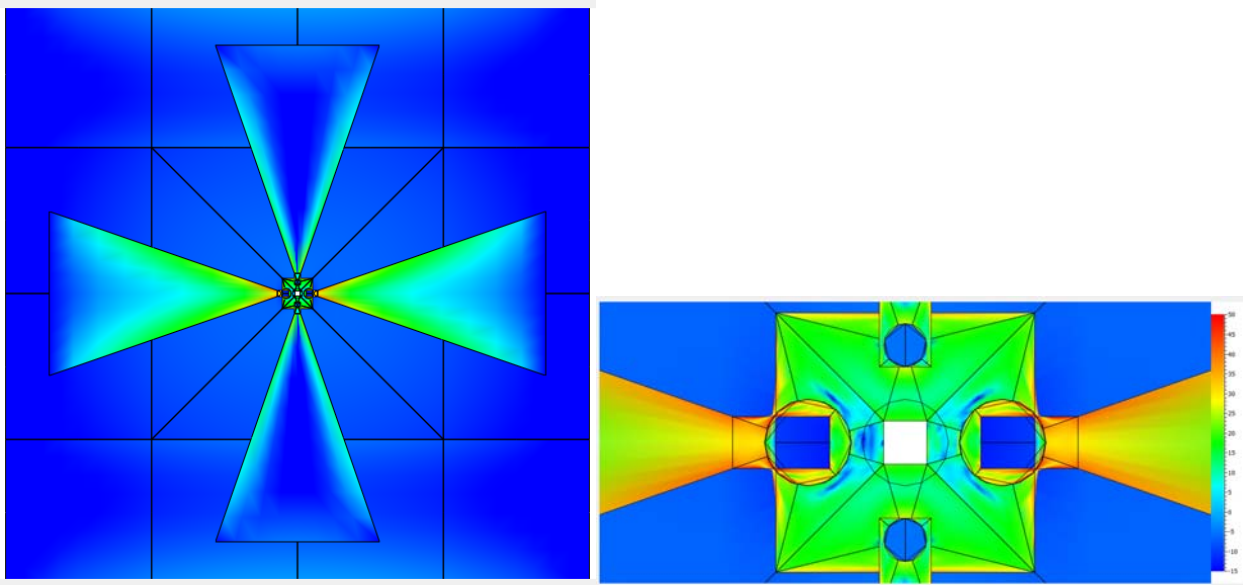

Fig. 16. Current magnitude maps from the GRASP calculations at 50 MHz. The left and right leafs are driven by a 50 ohm source and the top and bottom leafs are shorted to the circuit ground. The color scale is logarithmic in current density.

### 3.5 Comparison with LWA memo #178 analytical beam approximation

The original LWA beam calculations presumably used a similar configuration with a 3 m x 3 m ground shield and lossy ground. Figure 17 compares the GRASP results with the analytical approximation given LWA memo #178. The two beans agree at the 1 dB level or better over the 0 to 75 deg zenith angle range. The differences near the horizon could arise because the GRASP model had only a 30 m dia lossy ground. It should also be noted that the GRASP results which include the 45 deg azimuth cut show that the azimuthal variation in the beam deviates at the 10-20% level from being simply elliptical as is assumed in the LWA analytical approximations.

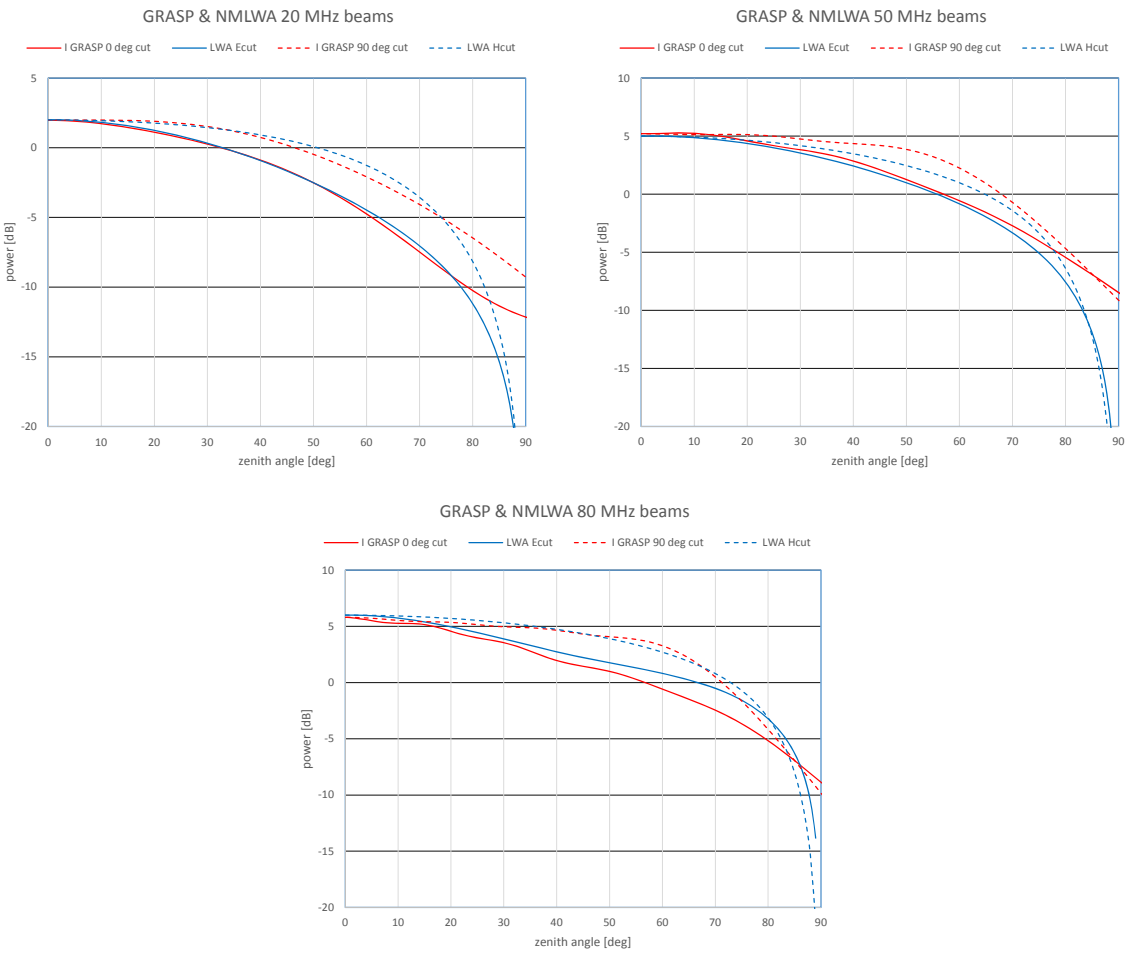


Fig. 17. Comparison of the GRASP calculations and analytic model for the LWA beam from LWA memo #178. The GRASP model is the same as plotted in figs. 11, 12 and 13. The LWA E-plane should be the same as the 0 deg azimuth plane and are plotted as blue and red solid lines. The H-plane and 90 deg azimuth plane cuts are plotted as dashed lines.

## 4. Effect of nearby antennas

One of the issues in array configuration is how close the closest pair of antennas should be. Closer spacing will increase the sensitivity to large scale or extended structure but close packing can distort the beam pattern. The LWA in New Mexico has a minimum spacing of 5 m between antennas. The OV-LWA has roughly the same number of antennas spread over four times the area, 200 m dia. circle instead of a 100 m circle. The OV-LWA configuration was scale from the NM-LWA by a factor of two and then optimized to give a better synthesized beam and to allow the shortest baselines to shrink back to 5 m.

GRASP was used to calculate the distortions of the beam of one station caused by a nearby station. Figure 18 shows the resulting 80 MHz beam pattern cut at an azimuth of 45 deg for a second antenna located 5 m away in the 45 deg azimuth direction. This figure shows changes in the beam that are periodic in zenith angle which is most likely the result of resonant interaction of the two antennas whose spacing is close the wavelength at 80 MHz. The peak change or deviation from the single antenna is 18% at a zenith angle of 20 deg. The change in beam shape as a function of frequency and its pseudo periodic structure will complicate the interpretation of wide-field spectral measurements using closely spaced antennas.

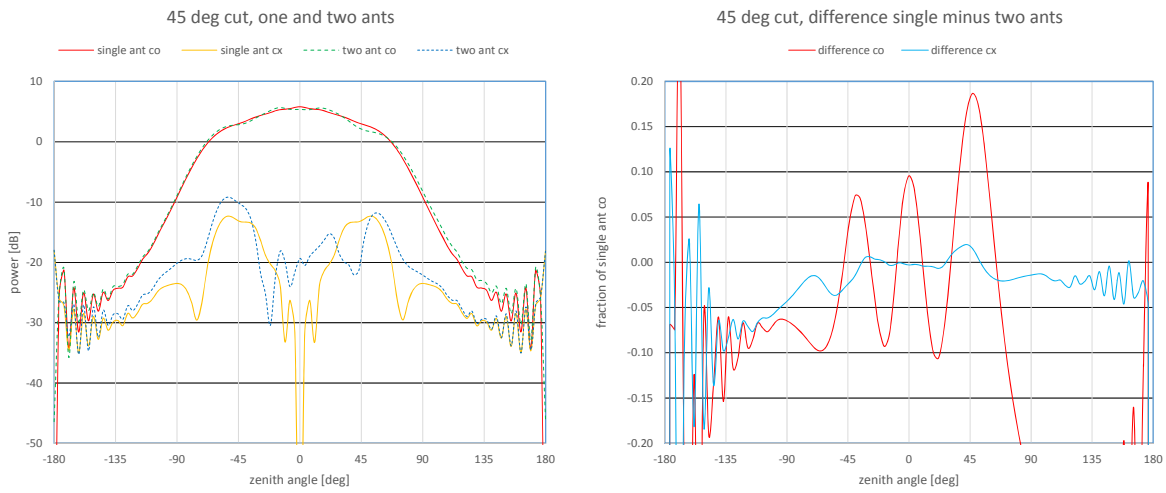


Fig. 18. Antenna beam at 80 MHz for an antenna and then with a second antenna stand located 5 m away along an azimuth of 45 deg. The left panel is the 45 deg beam cut. The right panel shows the fractional difference between and the single and two antenna beams powers divided by the single antenna beam power.

Figure 19 summaries the results for a series of calculations of the effect of nearby antennas at 20, 50 and 80 MHz for antenna separations of 3, 5 and 10 m. The RMS and peak deviation for both the nominal polarization and cross polarization are plotted. The most relevant plot for point source removal and fidelity is the peak deviations of the nominal polarization in the bottom left panel of fig. 19. This shows that the deviation of the antenna beam from nominal could be as large as 30% at 80 MHz for 5 m spacing and as large as 10% for 10 m spacing. The effect is somewhat less at the lower frequencies.

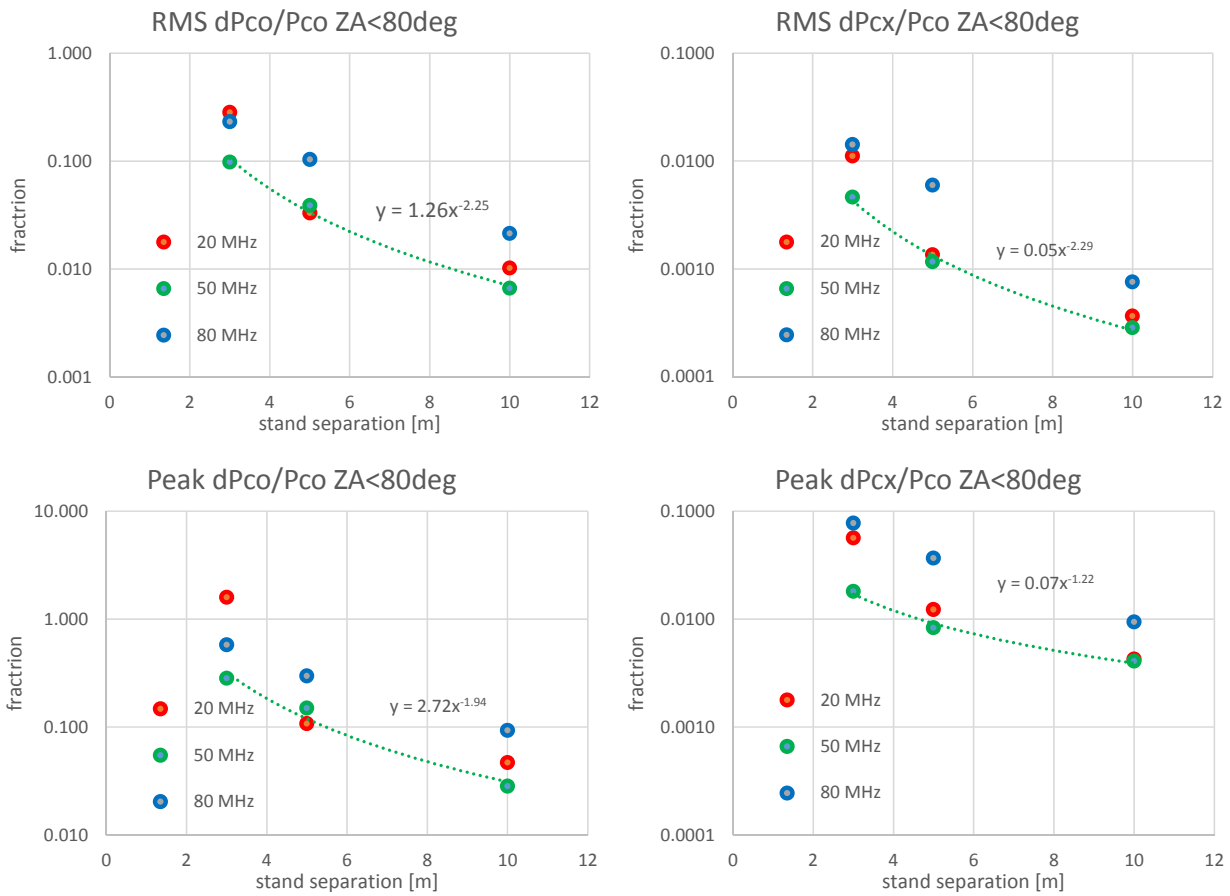


Fig. 19. Plots of the change in the beam pattern when a second antenna stand is placed nearby. These plots combine the data from the standard three beam cuts in azimuth (0, 45 and 90 deg) and for the second stand displaced a given distance from the first antenna in 0, 45, and 90 deg azimuth directions. The RMS plots are the RMS changes in the beam with the second antenna is nearby normalized by the single antenna beam over 0-80 zenith angles for all beam cuts and displacement directions. The peak values are the maximum change in the beam pattern over the same set of data.

The mutual coupling between closely spaced antenna stands can lead to false fringes that will effect wide-field images. The beams are calculated in the time reversed view, i.e. the antenna is analyzed as a radiator. Grasp does not provide a method for directly measuring the coupling to the neighboring antennas but the change in radiated power can be used as a rough proxy for the mutual coupling. The dipoles in the neighboring stand were terminated with shorts so they do not absorb any power but they can still couple to the antenna and change the impedance seen by the radiating antenna. Figure 20 shows a plot of the radiated power as a function of the stand separation. A crude estimate of the mutual coupling deduced from this plot is that at 3 m spacing the coupled power is on the order of -15 dB while at 5 m spacing it is -25 dB and at 10 m spacing -30 dB. There are two effects to consider; 1) noise emitted by one front end amplifier is coupled to the neighboring antenna and 2) radiation from the sky incident from the sky on one antenna is reflected back by the mismatch to the frontend amplifiers (note that the dipoles are poorly matched to the sky) and coupled to the neighboring antenna. Both effects produce false visibilities that will nominally be static as the earth rotates but they will have a spectral signature that will be hard to predict accurately. The second affect will have some time dependence as the brightest sources and the galactic plane pass overhead and also as the ionospheric emission changes. Even at -30 dB coupling, this is a fairly large effect for an

interferometer looking for weak signals and needs to be more accurately analyzed using a different MoM program that can more directly determine the mutual coupling.

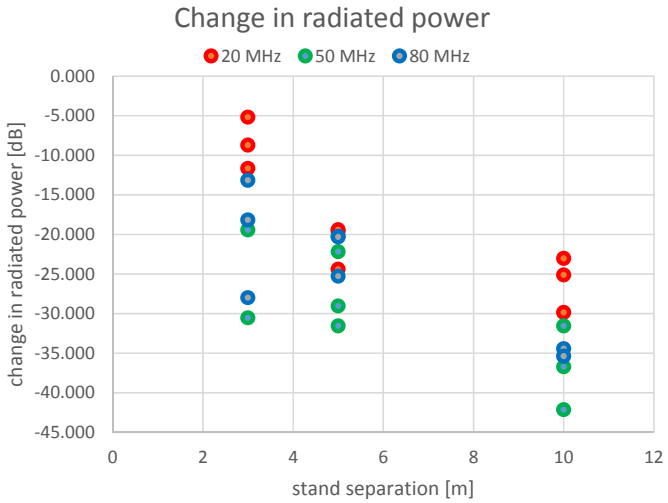


Fig. 20. The change in radiated power caused by placing a second antenna stand nearby. The three points at each separation and frequency are for the three orientations of the offset direction.

## 5. Summary and next steps

The simple LWA antennas are actually pretty complicated, especially when being utilized for interferometric measurements of weak polarized signals. The Stokes V and poor E-W to N-S polarization orthogonality present a significant calibration challenge. Close packing to measure large scale features is not too bad with 10 m spacing producing clean beams but 5 m spacing will require extra antenna specific beam calibration to make accurate images. About the only assumptions that hold up for mapping are that in the principle planes the polarization should be pretty linear with good polarization orthogonality between the E-W and N-S response and that the beams should be nearly the same for all antennas whose nearest neighbor is more than 10 m away. It should be possible to exploit the clean polarization in the principle planes for calibration as the sources move through these planes.

The calculations carried out using the GRASP and HFSS analysis packages show that most features in the beam are consistent but more work is required to achieve high fidelity agreement in the results. If the dominant features such as the Stokes V along the diagonal 45 deg azimuth plane and E-W to N-S polarization non-orthogonality are verified astronomically then it would be justified to work harder on the models to improve the agreement and between GRASP and HFSS models and improve their fidelity. It is reasonable to expect that the beam calculations could yield predictions that are accurate enough to use for good fidelity imaging in all Stokes parameters. It is not clear yet what angular and spatial resolution is required to accurately capture the beam parameters. At a minimum the calculations will point the way to what needs to be measured if a local direct beam measurement is attempted and what angular and frequency resolution is required to produce and astronomical calibration that can be applied over the full sky.